



## **Switchbacks in the Solar Magnetic Field: Their Evolution, Their Content, and Their Effects on the Plasma**

F. Mozer, O. Agapitov, S. Bale, J. Bonnell, T. Case, C. Chaston, D. W. Curtis, Thierry Dudok de Wit, K. Goetz, K. A. Goodrich, et al.

### **► To cite this version:**

F. Mozer, O. Agapitov, S. Bale, J. Bonnell, T. Case, et al.. Switchbacks in the Solar Magnetic Field: Their Evolution, Their Content, and Their Effects on the Plasma. *The Astrophysical Journal Supplement*, 2020, Early Results from Parker Solar Probe: Ushering a New Frontier in Space Exploration, 246 (2), pp.68. <10.3847/1538-4365/ab7196>. <insu-02884591>

**HAL Id: insu-02884591**

**<https://insu.hal.science/insu-02884591v1>**

Submitted on 30 Jun 2020

**HAL** is a multi-disciplinary open access archive for the deposit and dissemination of scientific research documents, whether they are published or not. The documents may come from teaching and research institutions in France or abroad, or from public or private research centers.

L'archive ouverte pluridisciplinaire **HAL**, est destinée au dépôt et à la diffusion de documents scientifiques de niveau recherche, publiés ou non, émanant des établissements d'enseignement et de recherche français ou étrangers, des laboratoires publics ou privés.



HAL Authorization



# Switchbacks in the Solar Magnetic Field: Their Evolution, Their Content, and Their Effects on the Plasma

F. S. Mozer<sup>1</sup> , O. V. Agapitov<sup>1</sup> , S. D. Bale<sup>1</sup> , J. W. Bonnell<sup>1</sup>, T. Case<sup>2</sup> , C. C. Chaston<sup>1</sup>, D. W. Curtis<sup>1</sup>, T. Dudok de Wit<sup>3</sup> , K. Goetz<sup>4</sup>, K. A. Goodrich<sup>1</sup>, P. R. Harvey<sup>1</sup>, J. C. Kasper<sup>5</sup> , K. E. Korreck<sup>2</sup> , V. Krasnoselskikh<sup>3</sup> , D. E. Larson<sup>1</sup>, R. Livi<sup>1</sup>, R. J. MacDowall<sup>6</sup> , D. Malaspina<sup>7</sup> , M. Pulupa<sup>1</sup> , M. Stevens<sup>2</sup> , P. L. Whittlesey<sup>1</sup> , and J. R. Wygant<sup>4</sup>

<sup>1</sup> University of California, Space Science Laboratory, Berkeley, CA, USA

<sup>2</sup> Smithsonian Astrophysical Observatory, Center For Astrophysics, Cambridge, MA, USA

<sup>3</sup> LPC2E, CNRS and University of Orléans, Orléans, France

<sup>4</sup> University of Minnesota, Minneapolis, MN, USA

<sup>5</sup> University of Michigan, Ann Arbor, MI, USA

<sup>6</sup> NASA/Goddard Space Flight Center, Greenbelt, MD, USA

<sup>7</sup> University of Colorado, Boulder, Laboratory for Atmospheric and Space Physics, Boulder, CO, USA

Received 2019 November 10; revised 2020 January 18; accepted 2020 January 28; published 2020 February 19

## Abstract

Switchbacks (rotations of the magnetic field) are observed on the *Parker Solar Probe*. Their evolution, content, and plasma effects are studied in this paper. The solar wind does not receive a net acceleration from switchbacks that it encountered upstream of the observation point. The typical switchback rotation angle increased with radial distance. Significant Poynting fluxes existed inside, but not outside, switchbacks, and the dependence of the Poynting flux amplitude on the switchback radial location and rotation angle is explained quantitatively as being proportional to  $(B \sin(\theta))^2$ . The solar wind flow inside switchbacks was faster than that outside due to the frozen-in ions moving with the magnetic structure at the Alfvén speed. This energy gain results from the divergence of the Poynting flux from outside to inside the switchback, which produces a loss of electromagnetic energy on switchback entry and recovery of that energy on exit, with the lost energy appearing in the plasma flow. Switchbacks contain 0.3–10 Hz waves that may result from currents and the Kelvin–Helmholtz instability that occurs at the switchback boundaries. These waves may combine with lower frequency magnetohydrodynamic waves to heat the plasma.

*Unified Astronomy Thesaurus concepts:* Solar magnetic fields (1503); Solar physics (1476); Solar wind (1534)

## 1. Introduction

An interesting result of the *Parker Solar Probe* mission has been the observation of switchbacks in the solar magnetic field. Switchbacks are seconds to minutes duration rotations of the magnetic field through angles that can be larger than 90°. The purpose of this paper is to discuss the evolution of switchbacks, their wave and plasma content, and their relationship to the acceleration of solar wind ions.

The *Parker Solar Probe* and its instruments are described elsewhere (Bale et al. 2016; Fox et al. 2016; Kasper et al. 2016). It is in a solar orbit with its first perihelion at 35 solar radii ( $R_\odot$ ) occurring on 2018 November 5 and its second perihelion at 35  $R_\odot$  occurring on 2019 April 5. The coordinate system used in the following discussion is tied to the spacecraft, has  $X$  perpendicular to the Sun–spacecraft line, is in the ecliptic plane, is pointing in the direction of solar rotation (against the ram direction), has  $Y$  perpendicular to the ecliptic plane, is pointing southward, and has  $Z$  pointing sunward. Figure 1 presents an overview of 10 days of fields and plasma data collected around the April perihelion. Figure 1(a) gives the  $Z$ -component of the magnetic field, which contains many spikes, which are the switchbacks (Bale et al. 2019; Kasper et al. 2019). Such structures were known prior to the *Parker Solar Probe* launch (Yamauchi et al. 2004; Suess 2007; Matteini et al. 2005, 2006, 2014; Borovsky 2016; Horbury et al. 2018). The

fact that the total magnetic field in Figure 1(e) was nearly devoid of variation as the switchbacks occurred shows that the switchbacks are primarily rotations of the magnetic field.

## 2. Data

To study the evolution of the switchbacks in time, Figure 2 presents the magnetic field rotation angle as a function of time for days near the  $\sim 35$  (actually 36.0)  $R_\odot$  perihelion and, five days earlier, at  $\sim 50$  (actually 48.2)  $R_\odot$ . To the eye, there appear to be more switchbacks at the outer radius, and they involved much larger field rotations than those at perihelion. This result is made quantitative in Figure 3, which gives the number of events with rotations greater than 30°, 60°, and 90° during the two days. The fact that there were many more switchbacks at the outer radius than at perihelion suggests that even fewer and smaller switchbacks occur closer to the Sun. Related statistical analyses on switchback occurrence are discussed in an accompanying article (Dudok de Wit et al. 2020).

As seen in Figure 1, switchbacks contain large Poynting fluxes (Figure 1(b), which gives the radial component of  $\mathbf{E} \times \mathbf{B}/\mu_0$ , where  $\mathbf{E}$  and  $\mathbf{B}$  are the electric and magnetic fields), energized ion kinetic energy (Figure 1(c), which gives  $0.5 m v^2$ , where  $v$  is the plasma bulk flow), and hotter radial plasma (Figure 1(d), which is  $0.5 m w^2$ , where  $w$  is the radial plasma thermal velocity). The Poynting flux of Figure 1(b) measures the  $Z$ -component of the electromagnetic energy, which was negative, meaning that the electromagnetic energy flowed away from the Sun, and it was spiky because the enhanced Poynting flux was embedded in magnetic field switchbacks. A striking



Original content from this work may be used under the terms of the [Creative Commons Attribution 4.0 licence](https://creativecommons.org/licenses/by/4.0/). Any further distribution of this work must maintain attribution to the author(s) and the title of the work, journal citation and DOI.

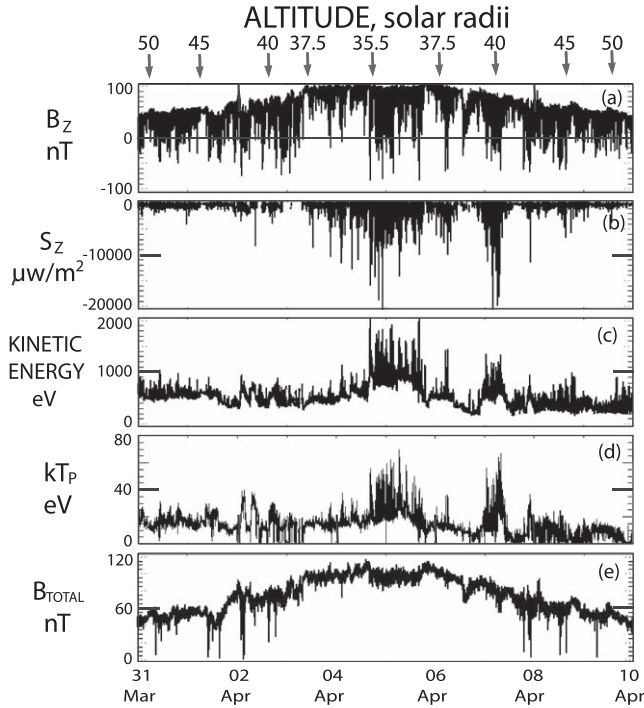


**Figure 1.** Field and particle measurements during 10 days of spacecraft passage through perihelion on 2019 April 4. Switchbacks in the magnetic field (Figure 1(a)) are associated with enhancements of the Poynting flux (Figure 1(b)) and increases of the solar wind kinetic energy and apparent temperature (Figures 1(c) and (d)).

feature of the Poynting flux is that it was large near perihelion and an order of magnitude smaller at  $50 R_{\odot}$ , both before and after perihelion. This same spatial dependence was observed over the same radial distances on the first perihelion pass, so these four observations are assumed to represent the spatial distribution of the Poynting flux. The proton kinetic energy of Figure 1(c) increased from 500 eV/particle to nearly 2000 eV/particle and the ion temperature of Figure 1(d) increased from 20 to 60 eV in regions of enhanced Poynting fluxes in switchbacks near perihelion.

Examples of switchbacks that illustrate these enhancements, at 35 and 50 solar radii, are given in Figure 4. Figures 4(c) and (k) give the radial components of the magnetic field whose value near perihelion at  $35 R_{\odot}$  changed from +100 to -90 nT, while at  $50 R_{\odot}$ , the field change was from 50 to 15 nT. These changes are characteristic of decreases of Poynting fluxes with distance and they identify these events as large amplitude switchbacks. Within the switchbacks, the largest Poynting flux was  $8000 \mu\text{W m}^{-2}$  at  $35 R_{\odot}$  (Figure 4(d)) and  $1000 \mu\text{W m}^{-2}$  at  $50 R_{\odot}$  (Figure 4(l)). The ion kinetic energy increased from 1000 to 3000 eV at  $35 R_{\odot}$  (Figure 4(e)) and from 500 to 600 eV at  $50 R_{\odot}$  (Figure 4(m)), while the radial ion temperature increased from 20 to 60 eV at perihelion (Figure 4(f)) and from 15 to 20 eV at  $50 R_{\odot}$ . During these times, the plasma densities (Figures 4(g) and (o)) and total magnetic fields (Figures 4(h) and (p)) remained roughly constant. These variations are characteristic of large switchbacks seen at the two radial distances.

Figures 4(a) and (i), and (b) and (j), present spectra of the perpendicular electric and magnetic fields, respectively. They show that the main power in the waves was at frequencies more than an order of magnitude below the  $\sim 1.5$  Hz ion gyrofrequency

or the Doppler-shifted ion inertial scale fluctuations (tens of Hz at these densities and solar wind speeds). They also show that such waves had much larger amplitudes at  $35 R_{\odot}$  than at  $50 R_{\odot}$ . This suggests that the waves were in the long wavelength Alfvén mode. Note that there was also wave power at 0.01–10 Hz inside the switchbacks, and these waves will be discussed below.

The next topic will be an investigation of the source and effects of the enhanced Poynting flux, ion bulk flow, and ion temperature. Figure 5 presents plots of the Poynting flux as functions of the magnetic field rotation angle at the two distances. It shows that the magnitude of the Poynting flux increased rapidly with the rotation angle of the switchbacks and was an order of magnitude larger at perihelion than at  $50 R_{\odot}$ . The absence of large Poynting fluxes in the dashed rectangles in Figure 5 shows that large Poynting fluxes were not present outside switchbacks.

The confinement of the Poynting flux to the interior of switchbacks is understood by realizing that, outside of the switchbacks, the radial solar wind flowed mostly parallel to the magnetic field. However, as the magnetic field rotates, more of the radial solar wind flow becomes perpendicular to the magnetic field, so it becomes an  $\mathbf{E} \times \mathbf{B}/B^2$  flow. Because the Poynting flux is  $\mathbf{E} \times \mathbf{B}/\mu_0$ , it must also increase along with  $\mathbf{E} \times \mathbf{B}/B^2$  as the magnetic field rotates.

One may obtain a quantitative expression for the Poynting flux as a function of the rotation angle and radial distance from the Sun in the following way. Because the solar wind speed is roughly constant between 35 and  $50 R_{\odot}$ ,  $\mathbf{E} \times \mathbf{B}/B^2$  at a fixed rotation angle is also constant. Thus,  $\mathbf{E} \times \mathbf{B}/\mu_0$  is proportional to  $B^2$ . At a magnetic field rotation angle,  $\theta$ , the component of velocity perpendicular to  $\mathbf{B}$  is proportional to  $\sin\theta$  and the component of this component along the radial direction is also  $\sin\theta$ . Thus, the Poynting flux as a function of the radial distance and magnetic field direction should be equal to  $K(B\sin\theta)^2$ , where  $K$  is a normalizing constant. The red curves in Figure 5 are plots of this function. Because they are consistent with the radial and angular variation of the Poynting flux, they suggest that the Poynting flux should increase rapidly at lower altitudes. However, because the magnetic field rotation likely decreases rapidly at lower altitudes (as suggested by Figure 2), this Poynting flux increase may not occur.

The variation of the ion flow velocity in switchbacks at 35 and  $50 R_{\odot}$  is illustrated in Figure 6 (also noted at larger solar radii by Matteini et al. 2014) in which the black dots are the total proton bulk speed and the red dots are the total magnetic field. The fact that the amplitudes of the red curves are independent of the magnetic field rotation angle shows that the field change was truly a rotation of the field.

Energized ions occur in switchbacks, as shown in Figures 1(c), 4, and 6. Because there are no more energetic ions inside the dashed rectangles of Figure 6, which are the locations where more energetic ions, created in upstream switchbacks, would appear in local regions that are outside of switchbacks, it is also evident that such ions are confined to the interiors of switchbacks.

To study the mechanism behind the increase of the ion velocity in switchbacks, the locally parallel and perpendicular velocities as functions of the magnetic field rotation are plotted in Figure 7 for the 24 hr when the *Parker Solar Probe* was at its  $35 R_{\odot}$  perihelion. As the magnetic field rotated to  $90^\circ$  inside switchbacks, the parallel (radial) velocity decreased to zero and the perpendicular (radial) velocity increased. At  $90^\circ$  rotation, the perpendicular speed was about  $600 \text{ km s}^{-1}$ , while at  $0^\circ$

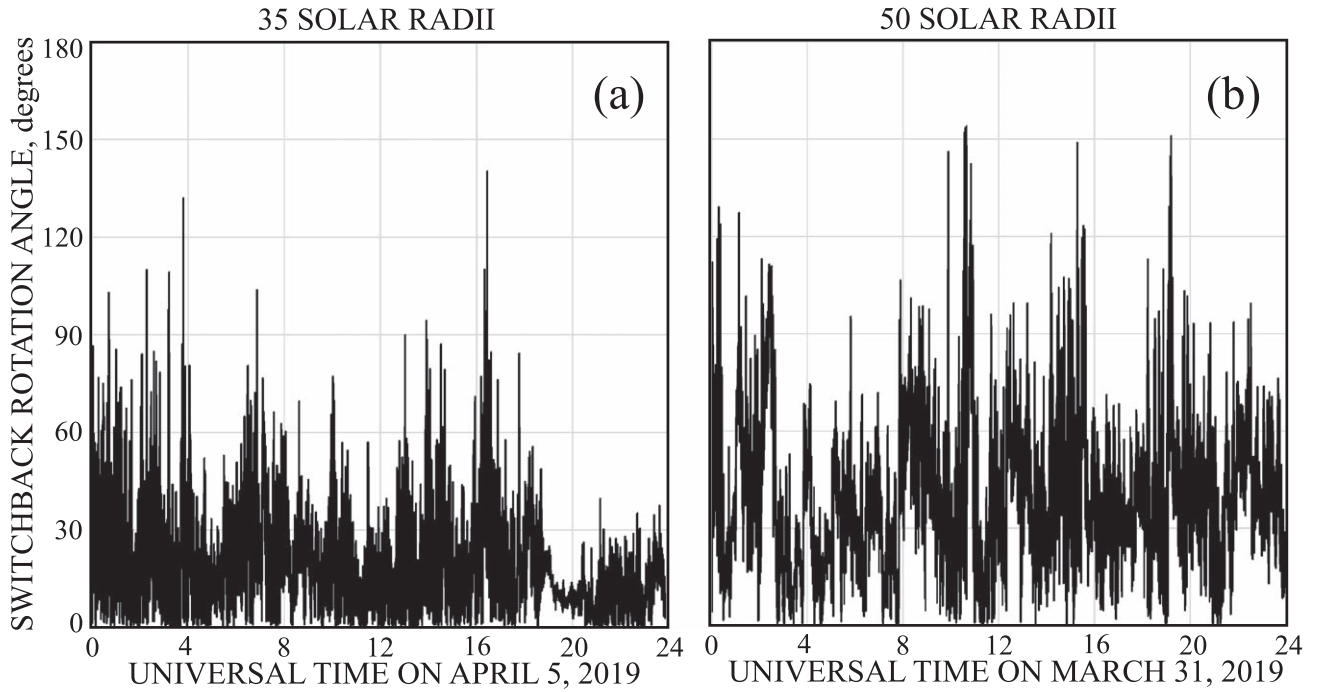


**Figure 2.** Switchback rotation angle as a function of time during one day intervals at the perihelion distance of 35 solar radii and at 50 solar radii.

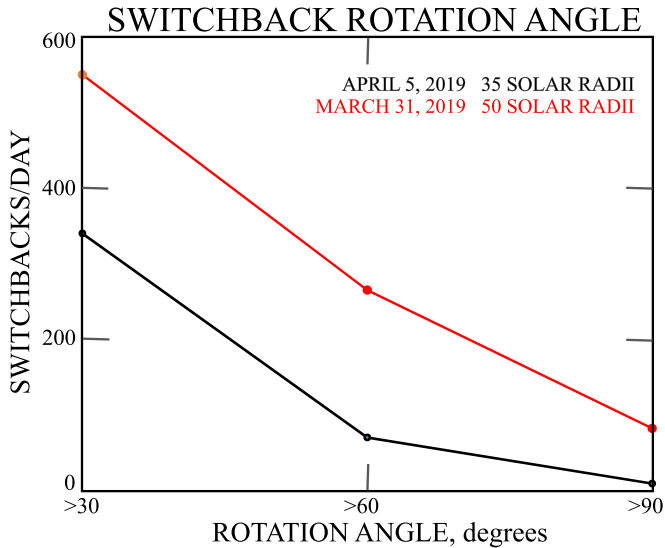


**Figure 3.** Number of switchbacks per day vs. their rotation angles at 35 and 50 solar radii. The increased number of large angle switchbacks at farther radial distances is illustrated.

rotation, the parallel speed was  $300 \text{ km s}^{-1}$ . This shows that there was a net increase of the total velocity as the magnetic field rotated. The perpendicular speed increased because it included the Alfvén speed associated with the magnetic field perturbation. Thus, the increased ion velocity inside switchbacks was caused by the frozen-in ion motion with the magnetic field as they both moved radially at the Alfvén speed. The plots in Figure 7 are curved. This is because they are proportional to the sine and cosine of the rotation angle, respectively.

The ion velocity in Figure 6(a) changed from about  $400$  to  $600 \text{ km s}^{-1}$  as the magnetic field rotated from  $0^\circ$  to  $90^\circ$  at perihelion. At  $50 R_\odot$ , the change in Figure 6(b) was from  $350$

to  $450 \text{ km s}^{-1}$ . The fact that the velocity change was a factor of  $\sim 2$  greater at  $35 R_\odot$  can be, at least partially, understood by the  $1/R$  decrease of the Alfvén speed between the two points, which is a factor of  $\sim 1.5$ .

The following discussion offers an answer to the question of where the ions got their additional energy inside the switchbacks. An overwhelming percentage of the Poynting flux in typical switchbacks is in the radial direction, so this is the component discussed in the following analysis in which it is assumed that the switchback and its ions are a static structure that advects across the spacecraft. The radial divergence of the Poynting flux,  $(\nabla \cdot \mathbf{S})$ , gives the change of electromagnetic energy across the divergence region according to Poynting's theorem. There is no divergence outside a switchback, from one side to the other, so there is no net electromagnetic energy gain or loss outside of the switchback and there is no solar wind energy change due to the switchback. However, there is a net divergence of the Poynting flux from outside to inside the switchback so there must be a loss of electromagnetic energy upon its entrance of the switchback and a nearly equal gain of electromagnetic energy upon its exit. These divergences result in the ions inside the switchback having a greater kinetic energy than those outside. This solar wind energy gain inside a typical switchback may be estimated by assuming that the solar wind velocity outside the switchback is  $400 \text{ km s}^{-1}$ , the density is  $80 \text{ cm}^{-3}$ , and the Poynting flux inside the switchback is  $6000 \mu\text{W m}^{-2}$ . For these values, the divergence of the Poynting flux results in a solar wind velocity gain of  $200 \text{ km s}^{-1}$  and the energy changes from  $830 \text{ eV}$  outside the switchback to  $1900 \text{ eV}$  inside. These results are in reasonable agreement with the observed changes of velocity and kinetic energy in Figures 6 and 7.

The increase of ion temperature inside switchbacks at the two radial distances is illustrated in Figure 8. This may be due to one or both of the following reasons. First, the temperature measurement is made only for the plasma component along the line of sight to the Sun. As the switchback rotates, the measured quantity changes from being the parallel temperature,



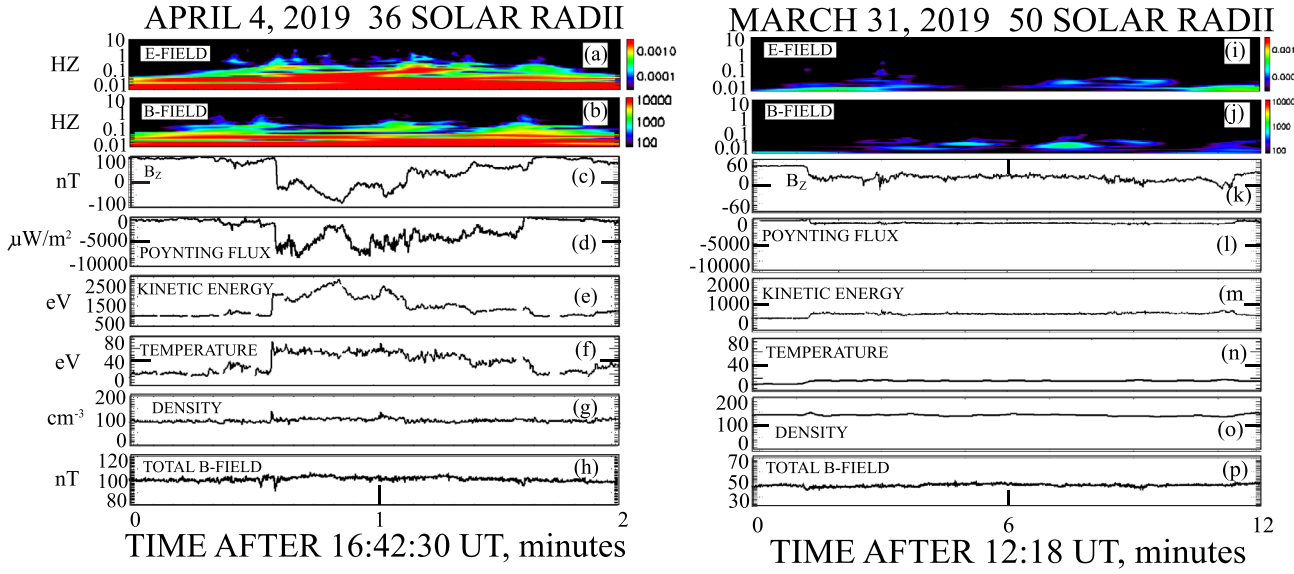


**Figure 4.** Wavelet spectra of the perpendicular electric field at 35  $R_{\odot}$  (Figure 4(a)) and 50  $R_{\odot}$  (Figure 4(i)), magnetic field wavelet spectra (Figure 4(b) and (j)), and plasma and field parameters at typical switchbacks. The wave power spectra peaked at the abrupt changes of the magnetic field. Because the wave power was at low frequencies and the total magnetic field did not change (Figures 4(h) and (p)), the waves were Alfvén mode waves. Also note the significantly greater variations of all parameters at 35  $R_{\odot}$  compared to 50  $R_{\odot}$ .

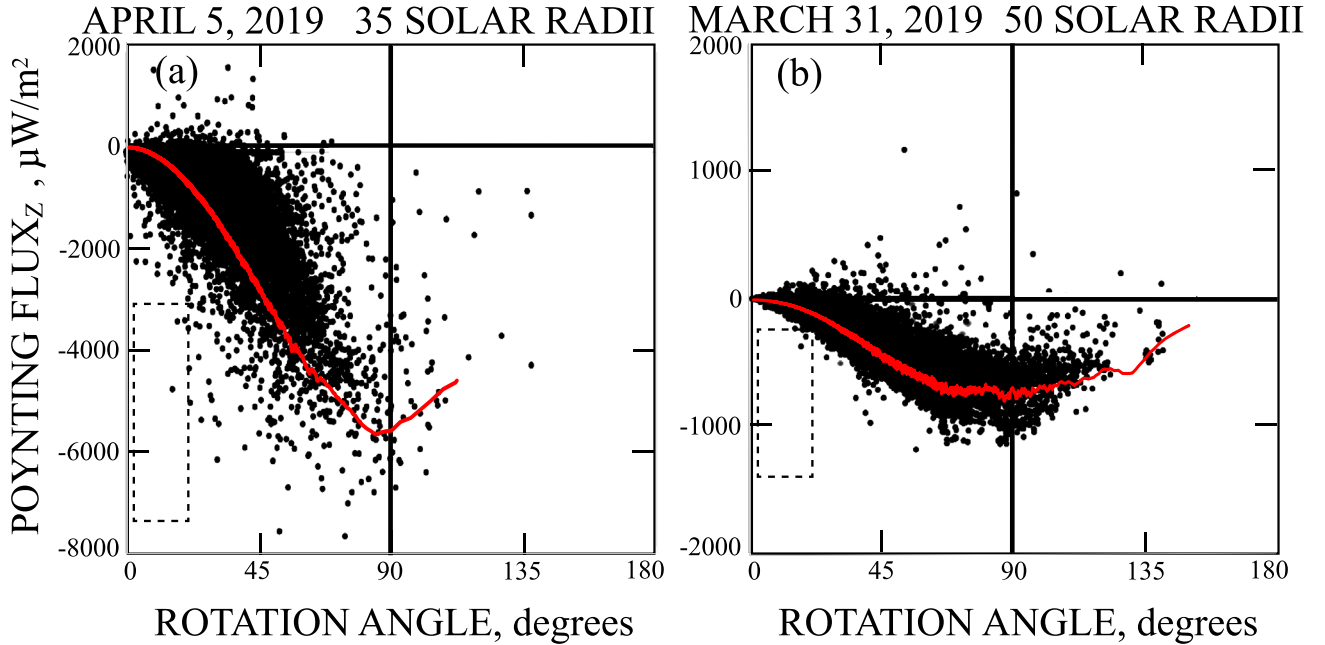


**Figure 5.** Radial Poynting flux as a function of the rotation angle of switchbacks at 35 and 50  $R_{\odot}$ . The angular range of switchback rotations was greater at 50  $R_{\odot}$  and the Poynting flux at 90° was an order of magnitude larger at 35  $R_{\odot}$  than at 50  $R_{\odot}$ . The red curves are equal to  $KB^2 \sin^2(\theta)$ , so they accurately describe the radial and angular dependencies of the Poynting flux. They also show why the Poynting flux was not significant outside switchbacks, i.e., inside the dashed rectangles.

$T_{\text{par}}$ , to the perpendicular temperature,  $T_{\text{perp}}$ . Thus, if  $T_{\text{perp}}/T_{\text{par}} > 1$ , the measured temperature would increase with the switchback rotation angle. Second, because of the waves discussed below, it is possible that the plasma is heated in the switchbacks. An ongoing analysis will attempt to distinguish between these two explanations. Note that the ion temperature at the outer radius is less than that at 35  $R_{\odot}$ . This is because the ions cool as they and the magnetic field expand.

Heating cannot be produced by long wavelength, low frequency Alfvénic turbulence alone, so additional waves must

be associated with switchbacks if there is heating. Such waves are present in the wavelet spectra of Figures 4(a) and (b) where the wave intensity at  $\sim 0.3$ –10 Hz is enhanced at the switchback boundaries and inside the switchbacks. Figure 9 presents expanded views at 35 and 50  $R_{\odot}$  of the  $\sim 0.3$ –10 Hz waves and turbulence in the data of Figure 4. Figures 9(a) and (d) present the three components of the magnetic field at the two locations with the changes of  $B_z$  indicating the switchback boundaries. Figures 9(b) and (e) present the fluctuations in the magnetic field with frequencies greater than 0.1 Hz, and Figures 9(c) and (f)

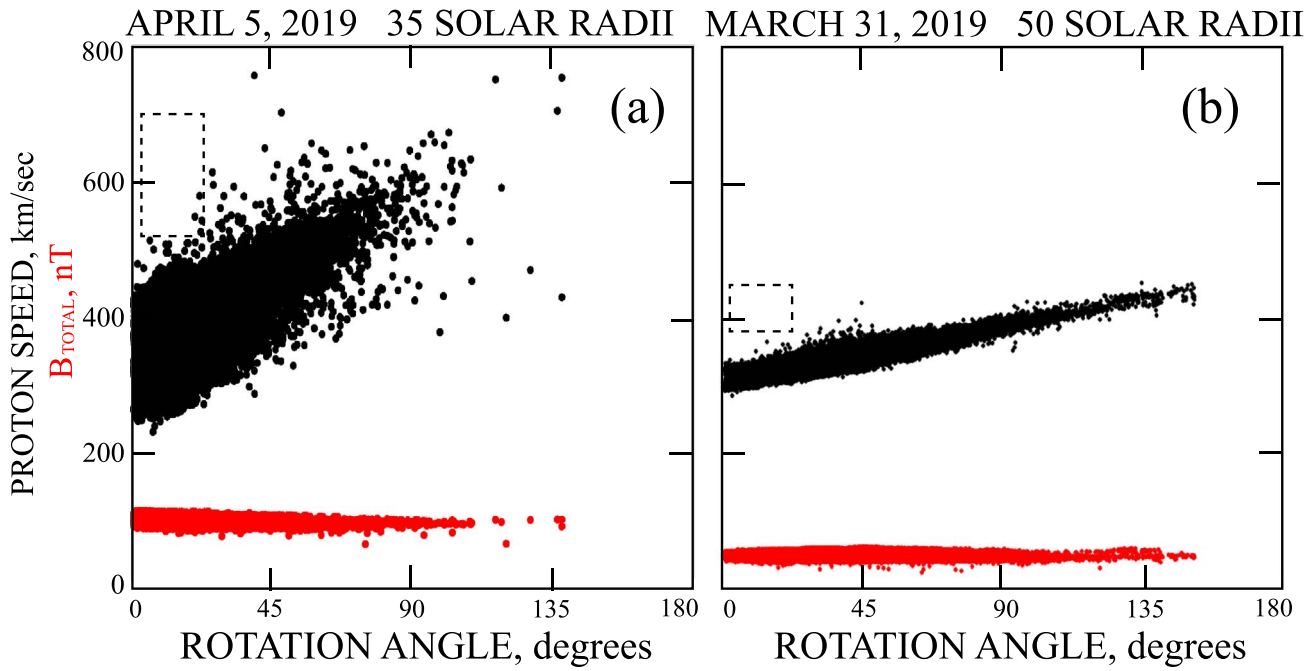


**Figure 6.** Proton bulk speed and the total magnetic field as functions of the switchback rotation angle at 35 and 50 solar radii. Because the total magnetic field did not vary with the rotation angle, the magnetic field variations must have been true rotations. The proton bulk speed is not enhanced outside of the switchbacks, i.e., inside the dashed rectangles.

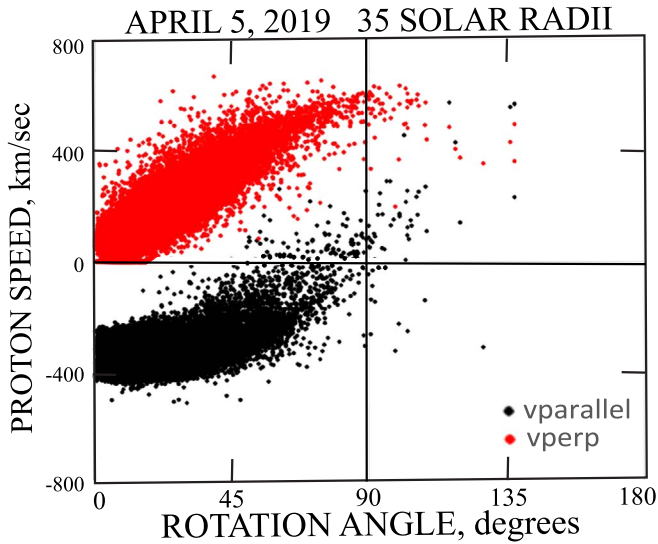


**Figure 7.** Local perpendicular and parallel components of the solar wind flow speed as functions of the magnetic field rotation angle. For zero rotation, the proton speed is parallel to the radial magnetic field while at 90° switchbacks, the radial flow is perpendicular to the local magnetic field, and it is larger than the flow speed outside of switchbacks (i.e., at zero degree rotations).

give their spectra at  $\sim 0.3$ –10 Hz. The amplitude of the fluctuations at 35  $R_{\odot}$  was about a factor of three greater than that at 50  $R_{\odot}$ .

Peaks in the spectra of Figures 4 and 9 occurred at the boundaries of the switchbacks, which suggests that waves were generated at these boundaries, as shown by Krasnoselskikh et al. (2020). Because the ion velocity inside the switchbacks was greater than that outside, it is feasible that the boundary was KH unstable and that this provided the source of these surface waves. To test this possibility, the fields were examined in the minimum variance coordinate system of the magnetic

field at each switchback boundary. The velocities at the beginning of the 35  $R_{\odot}$  switchback, near 16:43 UT and at its end, near 16:44 UT, show significant velocity shears (about  $260 \text{ km s}^{-1}$  and  $150 \text{ km s}^{-1}$ , respectively) with almost zero velocity along the normal direction. These boundaries would be unstable to the KH instability if the following inequality is satisfied (Miura 2003; Parks 2004):

$$\rho_1 \rho_2 [(\mathbf{v}_1 - \mathbf{v}_2) \cdot \mathbf{k}]^2 > (\rho_1 + \rho_2) [(\mathbf{B}_1 \cdot \mathbf{k})^2 + (\mathbf{B}_2 \cdot \mathbf{k})^2] / \mu_0, \quad (1)$$

where the subscripts refer to the two sides of a boundary,  $\rho$  is the mass density,  $\mathbf{k}$  is the wave vector,  $\mathbf{v}$  is the velocity, and  $\mathbf{B}$  is the magnetic field. For the wave normal vector directed along the velocity shear, this inequality is satisfied by a factor of  $\sim 2$  at the leading edge and 1.4 at the trailing edge of the switchback at 35  $R_{\odot}$ . Applying the same criteria to the data at 50  $R_{\odot}$  shows that this crossing was marginally stable.

There are two types of perturbations associated with the solar wind switchbacks: the large-scale Alfvénic perturbation associated with the rotation of the magnetic field and the small-scale waves inside the structure that are generated at the structure’s boundaries (Krasnoselskikh et al. 2020). The smaller-scale  $\sim 0.3$ –10 Hz waves are magnetohydrodynamic modes because their Doppler-shifted frequencies are below the ion cyclotron frequency of a few Hz. These perturbations affect the plasma in two ways: first, by the large-scale reversible enhancement of the plasma bulk velocity in the switchback and, second, by predominantly pitch angle scattering of the ions by the small-scale waves. This scattering of large bulk-velocity protons may spread part of the bulk flow kinetic energy and lead to heating of protons inside the switchback. Thus, the combined interactions of these different scale perturbations with protons may guide the transfer of switchback energy into thermal energy during the switchback propagation.

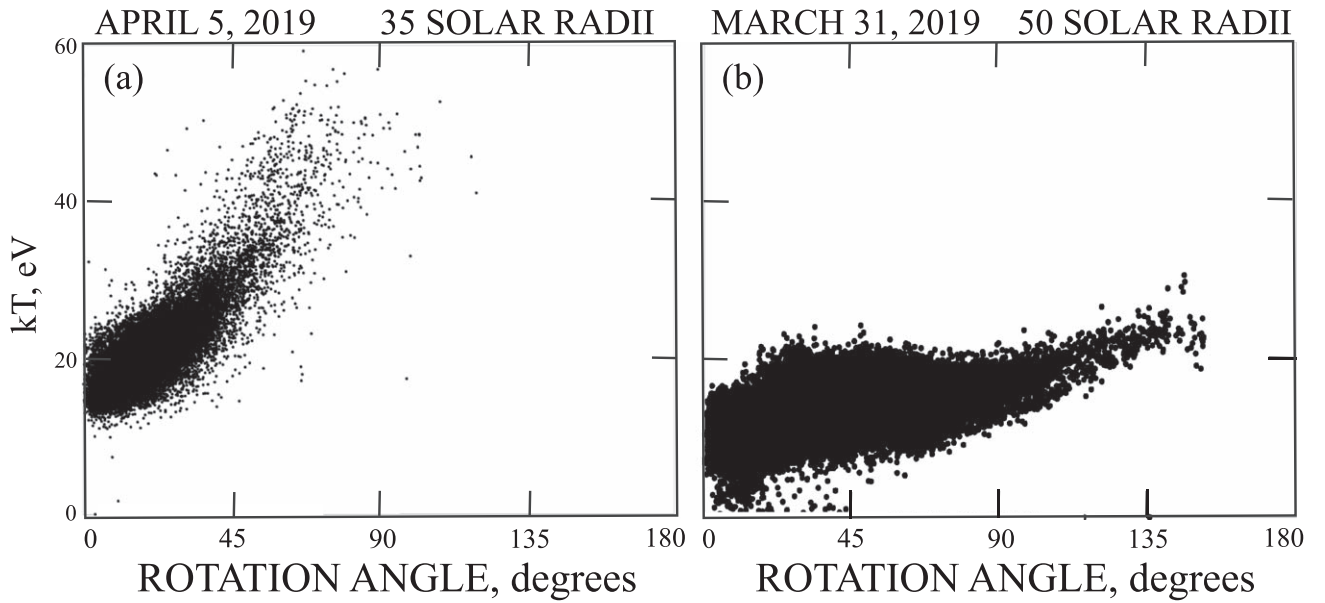


Figure 8. Ion temperature as a function of the switchback rotation angle.

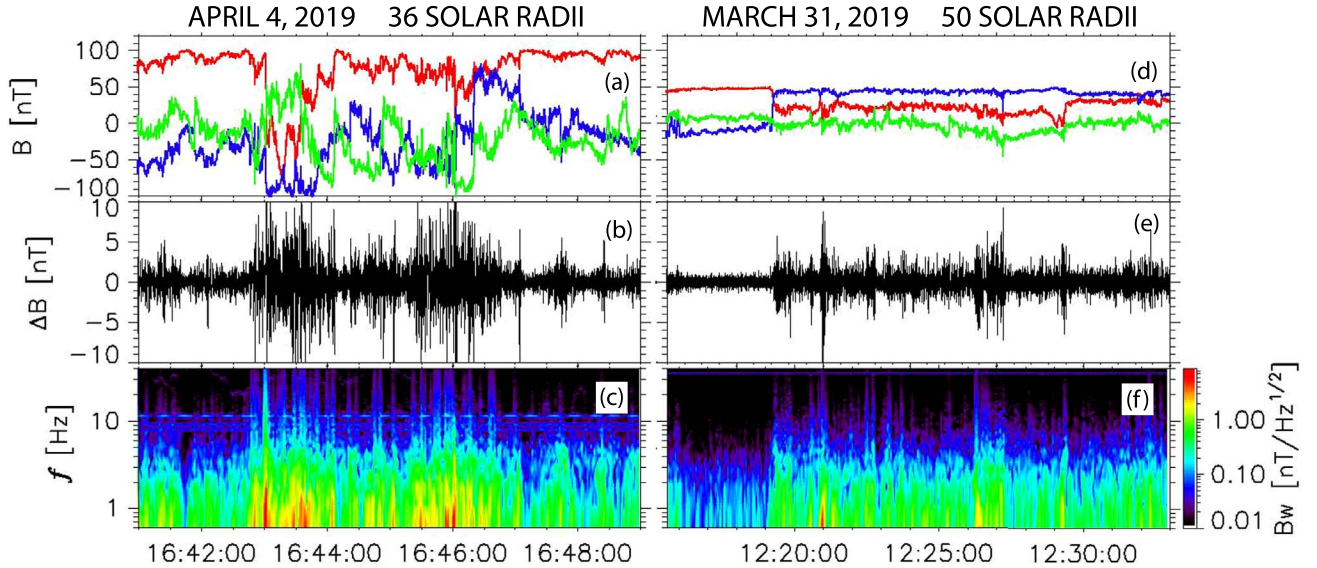


Figure 9. Magnetic field (Figures 9(a) and (d)), magnetic fluctuations (Figures 9(b) and (e)), and the magnetic field spectra (Figures 9(c) and (f)) during the switchbacks illustrated in Figure 4.

### 3. Summary

The switchback evolution in time and space has been studied with the conclusion that both the number of switchbacks per unit time and the magnetic field rotation inside them increase with the distance from the Sun. The switchbacks contained enhanced solar wind bulk flow, the Poynting flux, and thermal energy. The Poynting flux increased in switchbacks as a consequence of the rotation of the magnetic field such that the bulk flow changed from being parallel to the magnetic field to having a component perpendicular to the field. This perpendicular flow is  $\mathbf{E} \times \mathbf{B}/B^2$ . Hence,  $\mathbf{E} \times \mathbf{B}/\mu_0$ , the Poynting flux, also increased as the magnetic field rotated. For a fixed angular rotation, the Poynting flux varies with the radial distance from the Sun, as  $1/R^7$ . Thus, it is nearly an order of magnitude smaller at 50 solar radii than at 35 solar radii, as observed. This









radial dependence suggests the possibility that the Poynting flux is huge at smaller radii. This may be unlikely because the rotation angle also decreases at smaller radii. The Poynting flux outside switchbacks is essentially zero because the bulk flow is almost parallel to  $\mathbf{B}$ . Thus, the energy associated with the Poynting flux does not accelerate the bulk ion flow.

Even so, the bulk ion flow inside switchbacks was observed to increase relative to that outside. This is because the ions are tied to the oscillating magnetic field, so they gain an additional velocity proportional to the Alfvén speed, which they lose after the switchback passes by. This energy comes from the divergence of the Poynting flux of opposite signs upon entering and exiting the switchback. Because the Alfvén speed is proportional to  $1/R$ , the enhanced ion speed inside switchbacks is smaller at 50 solar radii than at 35 solar radii.

Wave power is observed at  $\sim 0.3\text{--}10$  Hz at the boundaries and inside switchbacks. These waves may result from large velocity shears at the switchback boundaries, which cause the boundaries to be Kelvin–Helmholtz (KH) unstable.

This work was supported by NASA contract NNN06AA01C. The authors acknowledge the extraordinary contributions of the *Parker Solar Probe* spacecraft engineering team at the Applied Physics Laboratory at Johns Hopkins University.

### ORCID iDs

F. S. Mozer  <https://orcid.org/0000-0002-2011-8140>  
 O. V. Agapitov  <https://orcid.org/0000-0001-6427-1596>  
 S. D. Bale  <https://orcid.org/0000-0002-1989-3596>  
 T. Case  <https://orcid.org/0000-0002-3520-4041>  
 T. Dudok de Wit  <https://orcid.org/0000-0002-4401-0943>  
 J. C. Kasper  <https://orcid.org/0000-0002-7077-930X>  
 K. E. Korreck  <https://orcid.org/0000-0001-6095-2490>  
 V. Krasnoselskikh  <https://orcid.org/0000-0002-6809-6219>  
 R. J. MacDowall  <https://orcid.org/0000-0003-3112-4201>  
 D. Malaspina  <https://orcid.org/0000-0003-1191-1558>

M. Pulupa  <https://orcid.org/0000-0002-1573-7457>  
 M. Stevens  <https://orcid.org/0000-0002-7728-0085>  
 P. L. Whittlesey  <https://orcid.org/0000-0002-7287-5098>

### References

- Bale, S. D., Badman, S. T., Bonnell, J. W., et al. 2019, *Natur*, 570, 232  
 Bale, S. D., Goetz, K., Harvey, P. R., et al. 2016, *SSRv*, 204, 49  
 Borovsky, J. E. 2016, *JGRA*, 121, 5055  
 Dudok de Wit, T., Krasnoselskikh, V., Bale, S. D., et al. 2020, *ApJS*, doi:10.3847/1538-4365/ab5853  
 Fox, N. J., Valli, M., Bale, S. D., et al. 2016, *SSRv*, 204, 7  
 Horbury, T. S., Matteini, L., & Stansby, D. 2018, *MNRAS*, 478, 1980  
 Kasper, J. C., Abiad, R., Auston, G., et al. 2016, *SSRv*, 204, 131  
 Kasper, J. C., Bale, S. D., Belcher, J. W., et al. 2019, *Natur*, 516, 228  
 Krasnoselskikh, V., Larosa, A., Agapitov, O., et al. 2020, *ApJ*, submitted  
 Matteini, L., Horbury, T. S., Neugebauer, M., et al. 2014, *GeoRL*, 41, 259  
 Matteini, L., Landi, S., Hellinger, P., & Velli, M. 2005, *ESA Spec. Publ.*, 592, 503  
 Matteini, L., Landi, S., Hellinger, P., & Velli, M. 2006, *JGRA*, 222, A10101  
 Miura, A. 2003, *JGR*, 108, 1076  
 Parks, G. K. 2004, *Physics of Space Plasmas; An Introduction* (Boulder, CO: Westview Press)  
 Suess, S. T. 2007, *ESA Spec. Publ.*, 641, 11  
 Yamauchi, Y., Suess, S. T., Steinberg, J. T., et al. 2004, *JGRA*, 109, 3104